Rheogenic Transport in the Renal Proximal Tubule

HENRY SACKIN and EMILE L. BOULPAEP

From the Department of Physiology, Yale University School of Medicine, New Haven, Connecticut 06510

ABSTRACT The electrophysiology of the renal Na-K ATPase was studied in isolated perfused amphibian proximal tubules during alterations in bath (serosal) potassium. Intracellular and extracellular ionic activity measurements permitted continuous evaluation of the Nernst potentials for Na^+, K^+, and Cl^- across the basolateral membrane. The cell membrane and transepithelial potential differences and resistances were also determined. Return of K to the basal (serosal) solution after a 20-min incubation in K-free solution hyperpolarized the basolateral membrane to an electrical potential that was more negative than the Nernst potential for either Na, Cl, or K. This constitutes strong evidence that at least under stimulated conditions the Na-K ATPase located at the basolateral membrane of the renal proximal tubule mediates a rheogenic process which directly transfers net charge across the cell membrane. Interpretation of these data in terms of an electrical equivalent circuit permitted calculation of both the rheogenic current and the Na/K coupling ratio of the basolateral pump. During the period between 1 and 3 min after pump reactivation by return of bath K, the basolateral rheogenic current was directly proportional to the intracellular Na activity, and the pump stoichiometry transiently exceeded the coupling ratio of 3Na to 2K reported in other preparations.

INTRODUCTION

The Na-K ATPase has been shown to mediate a rheogenic process in a variety of preparations, including erythrocytes (20), squid axons (11), snail neurons (58), skeletal muscle (26, 27, 40), and cardiac Purkinje fibers (18). In this paper, the term "rheogenic" is used throughout to denote a transport process that generates an electric current (from the Greek root "rheos" meaning stream or current). In this sense rheogenic transport is that subgroup of electrogenic processes that transfer net charge at the pump site itself via primary active ion transport (53).

In many epithelial tissues a Na-K pump is known to be located at the basolateral (serosal) cell membrane (13, 34, 56). However, it has generally been difficult to demonstrate unequivocally the rheogenic nature of these epithelial Na-K pumps. First, measurement of an ion flux across an epithelial

Address reprint requests to Dr. Henry Sackin, Dept. of Physiology, Cornell University Medical College, 1300 York Ave., New York, NY 10021.

J. GEN. PHYSIOL. © The Rockefeller University Press · 0022-1295/83/12/0819/33 $1.00

Volume 82 December 1983 819–851

cell membrane is complicated by the transport of that ion into or out of the cell across the contralateral membrane, as well as by ion movement via a paracellular route. This is true regardless of whether unidirectional isotopic fluxes are determined or whether net ionic fluxes are derived from changes in intracellular composition as measured by either chemical analysis or ion-selective microelectrodes. Second, even if the flux of Na or K can be accurately localized to the basolateral (serosal) cell membrane, it may be difficult to determine what fraction of that flux is passive and what fraction is due to the Na-K ATPase. Third, it should be emphasized that changes in cell membrane or transepithelial potentials after exposure to ouabain or K-free solutions do not in themselves constitute evidence for a rheogenic process since changes in electrical potential could arise simply from alterations in transmembrane ionic gradients produced by a neutral transport process.

In view of these difficulties, the present study attempts to assess the rheogenic nature of the renal Na-K pump using electrophysiological methods which require no assumptions about the detailed pathways of ion transport across the cell membranes. Specifically, the electrophysiology of the renal Na-K ATPase was studied in isolated perfused amphibian proximal tubules during removal and re-addition of bath (serosal) potassium. Measurement of intracellular and extracellular ionic activities permitted continuous evaluation of the Nernst potentials for Na^+, K^+, and Cl^-, as well as the total electromotive force across the basolateral membrane. The basolateral and transepithelial potential differences and resistances were also determined.

After a period of exposure to K-free bathing solution, return of K to the bath (serosal) side hyperpolarized the basolateral membrane to an electrical potential that was more negative than the Nernst potential for either Na, Cl, or K. This provides strong evidence that the Na-K ATPase located at the basolateral membrane of the renal proximal tubule directly generates a net current. Interpretation of these data in terms of an electrical equivalent circuit permitted calculation of both the rheogenic current and the Na/K coupling ratio of the basolateral pump.

METHODS

The detailed methods for dissection, isolation, and perfusion of amphibian proximal tubules have been extensively discussed in previous publications (50, 51). Only the main features are summarized below. Early proximal tubules between 500 and 900 μm in length were isolated from female neotenic salamanders (*Ambystoma tigrinum*) and perfused in vitro at rates of at least 20 nl/min. This perfusion rate was sufficient to ensure that the ionic composition of the perfusion fluid was not significantly modified by reabsorption along the length of the tubule. All experiments were performed at 22 ± 1°C.

Composition of Solutions

The compositions of the perfusion and bath solutions are summarized in Table I. All solutions were equilibrated with 1.5% CO_2/98.5% O_2. Since the solutions in Table I have essentially the same ionic strength, the individual ionic activity coefficients were assumed to be the same for solutions A, B, and C. Alterations in the K concentration

of the bathing solution were accomplished by equimolar exchange of K with Na. No albumin or colloids were used in the bath, but 1 g/liter Hercules green dye 1 (H. Kohnstamm & Co., New York) was added to the perfusion solution to assess the integrity of the tubular epithelium (50).

Measurements of Electrical Potentials and Resistances

The transepithelial potential difference, V_3, and the basolateral membrane potential difference, V_1, were measured as described previously (50, 51). Briefly, transepithelial potential differences were continuously monitored through both the perfusion and collection pipettes, which were connected to a dual electrometer (KS 700; W-P Instruments, Inc., Hamden, CT) via a Ringer-agar bridge and a Ag-AgCl electrode. Intracellular voltage-sensing electrodes of the Ling-Gerard type were fabricated from

TABLE I

Composition of Solutions

	A Control	B K free	C High K
Na^+	103.55	105.99	92.25
K^+	2.5	0.06	13.8
Ca^{++}	1.8	1.8	1.8
Mg^{++}	1.0	1.0	1.0
L-lysine H^+	0.2	0.2	0.2
Cl^-	94.7	94.7	94.7
HCO_3^-	10.0	10.0	10.0
$H_2PO_4^-$	0.5	0.5	0.5
$Lactate^-$	3.6	3.6	3.6
D-L-$glutamate^-$	0.05	0.05	0.05
D-glucose	2.22	2.22	2.22
D-L-alanine	0.5	0.5	0.5
L-glutamine	0.5	0.5	0.5

All solutions were equilibrated with 98.5% O_2 and 1.5% CO_2 and had a pH of 7.5. When solution A was used for luminal perfusion it contained 1 g/liter Hercules green dye 1.

microfiber capillary tubing (1 mm OD; Frederick Haer, Brunswick, ME) and filled with 3 M KCl by capillarity. Fig. 1 defines the direction with respect to the epithelium of the luminal (V_2), basolateral (V_1), and transepithelial (V_3) potential differences. The bath solution was maintained at ground. The average resistance and tip potential of the electrode were, respectively, 50–90 MΩ and 5–8 mV. Cells were impaled from the bath side and the basolateral membrane potential (V_1) was measured with a second dual electrometer (KS 700; W-P Instruments, Inc.) in contact with the KCl-filled microelectrode via a chlorided silver wire. The criteria for assessing the reliability of a particular microelectrode measurement have been previously discussed (51).

The methods for measurement of transepithelial resistance in isolated, perfused amphibian tubules have also been previously described (50). Namely, transepithelial resistance was determined by injecting square pulses of 100 nA and 10 s duration through the perfusion pipette and measuring the resulting voltage deflections at both the perfusion ΔV_3 ($x = 0$) and collection ΔV_3 ($x = L$) ends of the tubule. Representing the perfused proximal tubule as a terminated electrical cable, the length constant, λ, of the tubule is determined by:

$$L/\lambda = \cosh^{-1}[\Delta V_3\,(x = 0)/\Delta V_3\,(x = L)], \quad (1)$$

where L is the length of the tubule. Transepithelial resistance in Ωcm^2 epithelium is then given by Eq. 2:

$$R_{te} = 2\sqrt{\pi\lambda^3 R_{in} R_i}\ \sqrt{\tanh(L/\lambda)}, \quad (2)$$

where the input resistance, R_{in} (Ω), is defined as ΔV_3 ($x = 0$) divided by the total injected current. The volume resistivity, R_i (Ωcm), of each perfusion solution (A, B, and C, Table I) was measured with a conductivity meter (model CDM-2d; Radiometer, Copenhagen).

If the proximal tubule epithelium is represented as a double-core electrical cable (22, 57, 63), the individual cell membrane resistances are uniquely determined by two electrical parameters: (*a*) the parallel resistance of the cell layer, R_z (Ωcm^2), which is defined by the relation $1/R_z = 1/R_1 + 1/R_2$, and (*b*) the ratio of luminal to

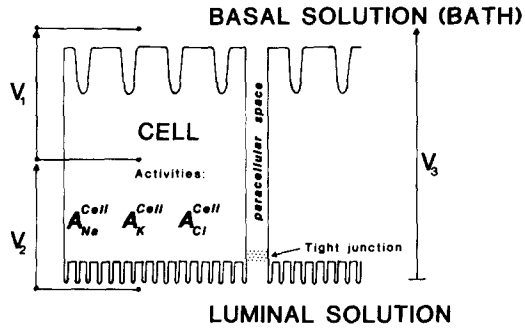

FIGURE 1. Schematic of a renal proximal tubule epithelial cell layer. The bath solution is maintained at ground potential. V_1 = basolateral cell membrane potential difference, V_2 = luminal cell membrane potential difference (cell minus lumen), and V_3 = transepithelial potential difference. The measured intracellular Na, K, and Cl ionic activities are respectively denoted by: a_{Na}^{cell}, a_K^{cell}, and a_{Cl}^{cell}.

basolateral membrane resistance, α ($= R_2/R_1$). The terms R_1 and R_2 denote, respectively, the basolateral and luminal cell membrane resistances. Since the cells of the amphibian proximal tubule are electrically coupled, injection of current into the epithelial cell layer produces an electrotonic voltage spread along the length of the tubule that is approximately an exponential function of the distance (x) from the current injection site. The magnitude of the voltage deflection, $V_{x,y=0}$, in cells parallel to the tubule axis and downstream from the current injection site at $x = 0$, $y = 0$ is described by Eq. 3, which applies to an infinite, double-core cable (22):

$$\ln V_{x,y=0} = \ln(R_z I_0/4\pi a\lambda_c) - (1/\lambda_c)x, \quad (3)$$

where λ_c is the cellular length constant of the tubule, I_0 is the total amount of current injected, a is the optically measured radius of the tubule, and R_z is the effective parallel resistance of the epithelial cell layer (22). Eq. 3 has been previously explained and derived in the appendix of reference 22 for the case of infinite-length tubules. The assumptions used to derive Eq. 3 should be equally valid for isolated perfused tubules as long as the current and voltage electrodes are at least several length

constants from either end of the tubule. This ensures that propagation of the injected current through the cell layer is essentially the same as for an infinite cable.

In practice, a semilog plot of voltage deflection ($V_{x,y=0}$) vs. distance (x) from the current injection site ($x = 0, y = 0$) determines the slope ($1/\lambda_c$) and intercept $\ln(R_z I_0/4\pi a\lambda_c)$ of Eq. 3. Since both I_0 and a can be independently measured for each tubule, the semilog plot uniquely specifies both λ_c and R_z. Estimates of the luminal to basolateral resistance ratio ($\alpha = R_2/R_1$) were obtained by simultaneous measurement of luminal and basolateral voltage deflections during passage of transepithelial current pulses. As described in reference 22, the value of α is approximately equal to the observed ratio of the luminal membrane to basolateral membrane voltage deflections resulting from transepithelial current injection. The values of R_z and α for a given tubule uniquely determine the individual cell membrane resistances, R_1 and R_2, according to Eqs. 4 and 5:

$$R_1 = R_z(1 + 1/\alpha); \tag{4}$$

$$R_2 = R_z(1 + \alpha). \tag{5}$$

Finally, it is possible to calculate the value of paracellular resistance (R_3) using R_{te}, α, and R_1:

$$R_3 = R_{te}(1 + \alpha)/(1 + \alpha - R_{te}/R_1). \tag{6}$$

Ion Activity Measurements

Intracellular sodium activity was measured with recessed-tip microelectrodes fabricated according to the technique of Thomas (59). Outer aluminosilicate glass microelectrodes were pulled on a two-stage vertical micropipette puller (model 700C; David Kopf Instruments, Tujunga, CA). Inner Na-selective microelectrodes were constructed from NAS 11-18 glass. The inner electrode was heat-sealed at the tip and then advanced close to the tip of the outer electrode, where it was fused to the inside of the aluminosilicate glass. The electrodes were filled with a solution of methanol saturated with NaCl, and electrical contact was made to a high-impedance dual electrometer (model FD223; W-P Instruments, Inc.) via a chlorided silver wire. The intracellular Na activity at any time t is described by Eq. 7, where V_{C-B}^{cell} denotes the difference between the cell Na electrode potential (V_C) and the potential (V_B) recorded by a 3 M KCl-filled electrode.

$$a_{Na}(t) = a_{Na}^{100\,mM\,NaCl} \cdot 10^{[V_{C-B}^{cell}(t) - V_{C-B}^{100\,mM\,NaCl}]/S} - k_{Na\text{-}K} a_K^{cell}. \tag{7}$$

The superscript designation "100 mM NaCl" indicates that the parameter was measured in pure 100 mM NaCl solutions. The slope (S) of a particular electrode was determined from the relation:

$$S = (V_C^{100\,mM\,NaCl} - V_C^{10\,mM\,NaCl})/0.94, \tag{8}$$

where 0.94 equals the logarithm (base 10) of the sodium activity ratio of pure 100 mM over pure 10 mM NaCl. The selectivity coefficient $k_{Na\text{-}K}$ appearing in Eq. 7 was computed from:

$$k_{Na\text{-}K} = \frac{a_{Na}^{100\,mM\,NaCl}}{a_K^{100\,mM\,KCl}} \cdot 10^{-[V_C^{100\,mM\,NaCl} - V_C^{100\,mM\,KCl}]/S}. \tag{9}$$

Since these electrodes had a Na-to-K selectivity of better than 200:1 ($k_{Na\text{-}K} \leq 0.005$), the net contribution of the term $k_{Na\text{-}K}a_K^{cell}$ in Eq. 7 will be negligible. Operationally, the intracellular Na activity was determined according to Eq. 7 by subtracting the basolateral membrane potential (V_B) measured with a 3 M KCl electrode from the potential recorded by a Na-selective electrode (V_C) that was located in a different cell of the same tubule. The justification for subtracting potential measurements from two different cells is that only small variations in basolateral membrane potential were observed between cells of the same tubule. Furthermore, within the same tubule there was <1 mV difference between basolateral membrane potentials recorded with a Ling-Gerard microelectrode and potentials recorded with an aluminosilicate micropipette filled with 3 M KCl (4).

Intracellular potassium activities were measured using double-barreled ion-selective microelectrodes with an overall tip diameter of slightly less than 1 μm (16, 30). The ion-selective side of the microelectrode was completely filled with potassium exchange resin (477317; Corning Medical and Scientific, Medfield, MA) and connected via a bare silver wire to channel A of a high-impedance electrometer (model F223A; W-P Instruments, Inc.). The reference barrel of the electrode was filled with 1 M NaCl and connected via a chlorided silver wire to channel B of the electrometer. Sodium chloride rather than potassium chloride was used to eliminate the possibility of leaking potassium into the vicinity of the K-sensing side of the electrode even though concentrated sodium chloride is more likely to result in tip potential changes during an impalement. Since the barrel of the electrode containing the exchanger records the sum of both the biological membrane potential and the electrode potential, intracellular potassium activity is calculated from the difference between the ion-selective potential, V_A, and the potential V_B, recorded by a 3 M KCl-filled electrode. This is indicated in Eq. 10, where $a_K^{cell}(t)$ is the time-dependent intracellular potassium activity and V_{A-B} equals $V_A - V_B$:

$$a_K^{cell}(t) = a_K^{100\,mM\,KCl} \cdot 10^{[V_{A-B}^{cell}(t) - V_{A-B}^{100\,mM\,KCl}]/S} - k_{K\text{-}Na}a_{Na}^{cell}(t). \quad (10)$$

The slope (S) of a particular electrode was determined from the relation:

$$S = (V_A^{100\,mM\,KCl} - V_A^{10\,mM\,KCl})/0.94, \quad (11)$$

where 0.94 is the base 10 logarithm of the ratio of K activities in a pure 100 mM KCl solution vs. a pure 10 mM KCl solution. The Na-to-K selectivity ($k_{K\text{-}Na}$) of the microelectrode was determined from Eq. 12, where it is implicitly assumed that the slope S of the microelectrode is a constant, independent of all ionic activities:

$$k_{K\text{-}Na} = \frac{a_K^{100\,mM\,KCl}}{a_{Na}^{100\,mM\,NaCl}} \cdot 10^{-[V_A^{100\,mM\,KCl} - V_A^{100\,mM\,NaCl}]/S}. \quad (12)$$

Standard 100 mM salt solutions (77 meq/liter activity) were used in order to mimic intracellular K^+ activities with an ionic strength similar to amphibian Ringer and presumably to intracellular composition as well. In general, these electrodes had a K-to-Na selectivity of better than 30:1 ($k_{K\text{-}Na} \leq 0.03$).

Intracellular Cl activities were measured with single-barreled chloride microelectrodes. Electrodes pulled from thick-walled aluminosilicate tubing (2 mm OD) were heated to 200°C for 2 h and silanized by a 2-min exposure to the evaporation of 10 μl of tri-*N*-butylchlorosilane in a covered 200-ml beaker. The cover was then removed and the electrodes were allowed to bake for an additional hour at 200°C. A small amount of chloride liquid exchanger (477315; Corning Medical and Scientific) was placed in the tip of the microelectrode and the rest of the electrode was filled with a

solution of 0.5 M NaCl. Electrical contact was made with the salt solution via a Ag-AgCl wire waxed into the back of the electrode. Intracellular Cl^- activity was determined by subtracting the cell membrane potential (V_B), measured with a 3 M KCl electrode, from the potential recorded by a Cl-selective electrode (V_D) that was placed in a different cell of the same tubule. The intracellular Cl^- activity at any time t is given by:

$$a_{Cl}^{cell}(t) = a_{Cl}^{100\,mM\,NaCl} \cdot 10^{[V_{D-B}^{cell}(t) - V_{D-B}^{100\,mM\,NaCl}]/S} - k_{Cl\,HCO_3} \cdot a_{HCO_3}^{cell}, \quad (13)$$

where V_{D-B} denotes the difference in electrical potential between the Cl^--selective electrode potential (V_D) and the potential (V_B) recorded with the 3 M KCl-filled electrode. The slope S of a particular electrode was determined from Eq. 8, using solutions of pure 100 mM NaCl and pure 10 mM NaCl. The Cl^--to-HCO_3^- selectivity, $k_{Cl\text{-}HCO_3}$, of the microelectrode was determined from Eq. 14, where it was assumed that the slope S of the microelectrode is constant:

$$k_{Cl\text{-}HCO_3} = \frac{a_{Cl}^{100\,mM\,NaCl}}{a_{HCO_3}^{100\,mM\,NaHCO_3}} \cdot 10^{-[V_D^{100\,mM\,NaCl} - V_D^{100\,mM\,NaHCO_3}]/S}. \quad (14)$$

Finally, the time course of the Na, K, and Cl Nernst equilibrium potentials across the basolateral cell membrane were calculated from the intracellular and extracellular ionic activities according to Eq. 15, where j represents either Na, K, or Cl, and z_j is the valence of ion j:

$$E_j = -\frac{RT}{z_j F} \ln \frac{a_j^{cell}(t)}{a_j^{bath}(t)}. \quad (15)$$

Experimental Procedure

After a 10–20-min period of equilibration with control solutions lumen and bath (solution A, Table I), the bath was replaced by a solution that was essentially free of K (solution B, Table I). Tubules were maintained under these zero-K conditions for 20 min, at which time the bath was rapidly replaced with a solution containing a higher than normal K concentration (solution C, Table I). During a change from solution B to solution C, ~90% of the bath could be replaced in ~4 s, as determined by measurement of extracellular K activities using K-selective microelectrodes. This estimate assumes that the response time of the K-selective liquid ion exchanger electrode is much less than 4 s. During a similar rapid alteration of the bathing solution from pure 100 mM KCl (0 meq/liter sodium activity) to a solution of 86 mM KCl and 14 mM NaCl (11 meq/liter sodium activity), the recessed-tip Na electrodes recorded 90% of the steady state signal in 10–15 s. Hence, at the same rate of bath exchange the Na-selective glass electrodes were ~6–11 s slower at registering a similar step in concentration.

The transepithelial potential difference (V_3) and resistance (R_{te}), as well as basolateral membrane potential (V_1), were measured throughout the experimental protocol. With respect to intracellular activities, the potential of an intracellular Na-selective electrode was continuously recorded during the control period, at the time of low bath K, and for 5 min during restoration of K to the bathing solution. A recording of the basolateral membrane potential of an adjacent cell was obtained simultaneously. The difference between these two potentials was read from the records at selected times and used to calculate a_{Na} in the cell at those times. This was repeated for five tubules. The average a_{Na}^{cell}'s were calculated for each selected time and are listed in Table II.This procedure was repeated on seven other tubules using

TABLE II

Ionic Activities and Electrical Potentials During Removal and Re-Addition of Bath Potassium

Experimental condition	Bath and cell ionic activities (meq/liter)*						Basolateral Nernst potentials (mV)			Basolateral and transepithelial potentials (mV)	
	a_{Na}^{bath}	a_{K}^{bath}	a_{Cl}^{bath}	a_{Na}^{cell}	a_{K}^{cell}	a_{Cl}^{cell}	E_{Na}	E_K	E_{Cl}	V_l	V_s
Control	80	2	73	21.4±1 (n = 7)	54.7±3 (n = 14)	15.3±3 (n = 6)	34.5	−85.4	−40.8	−63.6±3 (n = 14)	−4.5±0.5 (n = 14)
20 min of zero-K bath	82	0.05	73	68.1±4 (n = 7)	22.2±2 (n = 14)	28.9±4 (n = 6)	4.8	−157.2	−23.8	−20.7±1 (n = 14)	−0.9±0.2 (n = 14)
10 s after 11 K^+ bath	70.6±7 (n = 5)	10.3±2 (n = 7)	73	67.5±5 (n = 5)	27.5±2 (n = 7)	28.0±3 (n = 5)	1.3	−23.6	−24.7	−44.1±2 (n = 7)	−2.0±0.4 (n = 7)
30 s after 11 K^+ bath	70.6±5 (n = 5)	10.7±3 (n = 7)	73	63.7±7 (n = 5)	32.6±2 (n = 7)	26.0±4 (n = 5)	2.7	−28.3	−26.6	−51.7±2 (n = 7)	−2.5±0.5 (n = 7)
1 min after 11 K^+ bath	71	10.7	73	61.2±8 (n = 5)	39.2±2 (n = 7)	25.1±4 (n = 5)	3.8	−32.8	−27.7	−55.0±3 (n = 7)	−2.9±0.6 (n = 7)
1.5 min after 11 K^+ bath	71	11	73	48.6±8 (n = 5)	44.1±1 (n = 7)	24.5±3 (n = 5)	9.8	−35.8	−28.2	−53.3±3 (n = 7)	−3.0±0.5 (n = 7)
2 min after 11 K^+ bath	71	11	73	40.8±8 (n = 5)	51.4±1 (n = 7)	24.0±3 (n = 5)	14.3	−39.8	−28.7	−49.1±2 (n = 7)	−3.0±0.6 (n = 7)
3 min after 11 K^+ bath	71	11	73	26.9±5 (n = 5)	57.2±2 (n = 7)	23.1±4 (n = 5)	25.0	−42.5	−29.8	−41.1±2 (n = 7)	−2.9±0.6 (n = 7)
4 min after 11 K^+ bath	71	11	73	20.9±4 (n = 5)	59.3±2 (n = 7)	22.0±3 (n = 5)	31.6	−43.5	−30.9	−40.2±2 (n = 7)	−3.0±0.6 (n = 7)
5 min after 11 K^+ bath	71	11	73	16.3±3 (n = 5)	61.4±2 (n = 7)	21.1±4 (n = 5)	38.0	−44.4	−32.2	−39.1±3 (n = 7)	−3.0±0.7 (n = 7)

* The values of ionic activity followed by standard errors and the number of tubules (n) were measured directly with ion-selective electrodes. The values of activity with no standard errors were computed from the chemical concentration of the solute using the appropriate activity coefficient for that ion.

a double-barreled K-selective microelectrode and yielded the calculated average a_K^{cell} values listed in Table II. Similar measurements on five other tubules using a single-barreled Cl-selective electrode and an adjacent voltage electrode provided the calculated average a_{Cl}^{cell} values in Table II. Fig. 2 was constructed using the average values of the variables from Table II. On the other hand, individual luminal (R_2) and basolateral (R_1) membrane resistances were measured only during control conditions. Deviations from these control resistances resulting from alterations in bath K were calculated as described in the Discussion.

Throughout the experimental procedure the tubule lumen was rapidly perfused with the standard control solution (A, Table I). In preliminary experiments, the

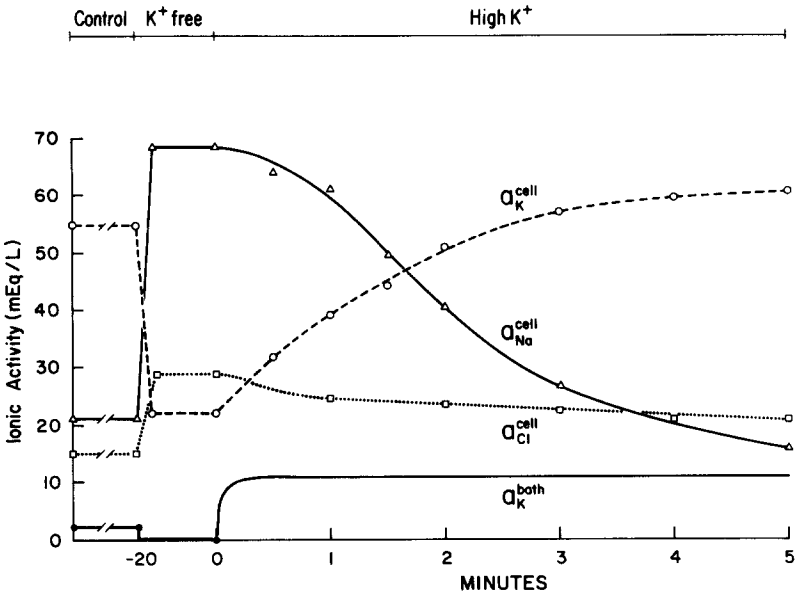

FIGURE 2. The effect of basolateral potassium removal and re-addition on intracellular sodium (△), potassium (○), and chloride (□) activities in the salamander proximal tubule. The bottom tracing indicates the potassium activity in the bathing (serosal) solution. Before time zero, the bath solution was maintained essentially K-free for 20 min. The time course of the intracellular activities during both control and K-free periods is greatly compressed. At time zero on the abscissa, bath K activity is abruptly increased to 11 meq/liter and maintained at this level. The plotted points are calculated averages from Table II and the intracellular activity curves were fitted by eye to the points.

above sequence of changes in bath K was conducted with K absent from the lumen. Electrical parameters measured under these conditions were not significantly different from those reported in the Results. Hence, the effect of changes in bath K on a paracellular K diffusion potential must be quite small.

All results are presented as mean values ± SE with n equal to the number of tubules. Statistical comparisons were made with the paired t test unless otherwise indicated.

RESULTS

Control Values

Table III summarizes the normal electrical potentials, resistances, and intracellular ionic activities for the group of salamander proximal tubules used in this study. The average basolateral membrane potential (V_1) of −64.4 mV and the average transepithelial potential (V_3) of −4.2 mV are similar to values of electrical potential that have been previously reported for in vivo *Necturus* proximal tubules (6), as well as for isolated perfused *Ambystoma* proximal tubules (51). The luminal cell membrane potential difference (V_2), defined as the potential in the lumen minus the potential in the cell, is obtained by

TABLE III

Control Electrical Parameters and Intracellular Ionic Activities

Basolateral membrane potential difference	V_1 (mV)	−64.4±2	(n = 32)
Luminal membrane potential difference	V_2 (mV)	+60.2±2	(n = 32)
Transepithelial potential difference	V_3 (mV)	−4.2±0.3	(n = 32)
Transepithelial resistance	R_{te} (Ωcm^2)	63.6±8	(n = 7)
Ratio of luminal to basolateral cell membrane resistance	α (= R_2/R_1)	2.9±0.2	(n = 8)
Length constant of the cell cable	λ_c (μm)	294.2±69	(n = 5)*
Parallel resistance of apical and basolateral membranes	R_z (Ωcm^2)	443.6±44	(n = 5)*
Basolateral cell membrane resistance	R_1 (Ωcm^2)	591.6±58	(n = 5)
Luminal cell membrane resistance	R_2 (Ωcm^2)	1774.2±174	(n = 5)
Paracellular resistance	R_3 (Ωcm^2)	65.5±0.2	(n = 5)
Intracellular Na activity	a_{Na}^{cell} (meq/liter)	21.4±1	(n = 7)
Intracellular K activity	a_{K}^{cell} (meq/liter)	54.7±3	(n = 14)
Intracellular Cl activity	a_{Cl}^{cell} (meq/liter)	15.3±3	(n = 6)

* The injected current (I_0) for the cell cable measurements was a square pulse of 50 nA and 10 s duration. The mean inner diameter for this group of five tubules was 80.6 μm.

electronic subtraction of V_1 from V_3 and hence is not an independently measured parameter.

In those tubules where transepithelial resistance was measured, the average observed value of 63.6 Ωcm^2 is somewhat higher than previously reported values of 52.1 Ωcm^2 for isolated perfused proximal tubules of *Ambystoma* (50). In addition, the approximate ratio of luminal to basolateral cell membrane resistance determined under control conditions for eight tubules is 2.9 compared with previous estimates of 3.9 (50). However, as discussed in reference 8, the value of 2.9, determined from the ratio of luminal to basolateral voltage deflections, represents a minimum estimate of $\alpha = R_2/R_1$. The distributed nature of the interspace and lateral membrane resistance requires that the actual ratio R_2/R_1 be slightly larger than the observed voltage deflection ratio. Nonetheless, the value of α = 2.9 is similar to the resistance ratios calculated for doubly perfused *Necturus* proximal tubules ranging from 2.5 to 2.9 (6, 22).

Individual cell membrane resistances were determined in five isolated perfused *Ambystoma* proximal tubules by recording basolateral voltage deflections at two distances from an intracellular current-injection electrode. The microelectrodes were placed at sufficient distances from the ends of the tubule to allow use of the nonterminated, double-core cable equations (22). The cell resistance measurements were performed using elevated transmural pressures in order to achieve the largest possible ratio of luminal diameter to cell thickness. This ensures a two-dimensional spread of current throughout the cylindrical layer of cells with negligible current flow along the radial axis of the tubule. As a result, the average luminal diameter of 80.6 μm is considerably larger than what is observed at normal perfusion pressures. Cell resistance data for five isolated perfused proximal tubules are summarized in the middle section of Table III. The average length constant and parallel resistance of the epithelial cell layer were, respectively: λ_c = 294 μm and R_z = 444 Ωcm^2. Since the average length constant for transepithelial current injection (during measurement of R_{te}) was only λ = 241 μm, current that leaks into the lumen from an intracellular microelectrode will reach the bath largely via the paracellular path. As a result, only a minuscule amount of intracellularly injected current will re-enter the cell from the tubule lumen and the problem of cross talk between luminal and cellular cables will be negligible (22). This eliminates a major source of error in the use of a double-core cable representation for the proximal tubule. Table III summarizes the values of electrical resistance R_1, R_2, and R_3, which have been calculated from Eqs. 4–6 for the case of identical substrate Ringer solutions (A, Table I) in lumen and bath.

For comparison, the length constant and parallel resistance of the epithelial cell layer in doubly perfused *Necturus* proximal tubules were, respectively: λ_c = 248 μm and R_z = 1,784 Ωcm^2 (22). Although *Ambystoma* and *Necturus* proximal tubules have similar cellular length constants (λ_c), *Necturus* parallel resistance (R_z) and cell membrane resistances (R_1, R_2) are approximately four times larger than the corresponding resistances for *Ambystoma* proximal tubules. The lower electrical resistance per square centimeter of epithelium of *Ambystoma* vs. *Necturus* tubules is consistent with the more extensive amplification of *Ambystoma* luminal and basolateral membrane area (39, 52). Despite differences in absolute electrical resistance, the proximal tubules of both *Necturus* and *Ambystoma* can be classified as leaky epithelia, since in both preparations the sum of luminal and basolateral cell membrane resistance is ~35 times the paracellular resistance.

Under control conditions, the mean intracellular Na activity of isolated perfused *Ambystoma* proximal tubules was 21.4 meq/liter. This is similar to values of ~24 meq/liter, which have been previously reported for this same preparation (4, 48, 51), as well as values of 22 meq/liter measured in bullfrog proximal tubules (17) and 20.0 meq/liter measured in blood-perfused *Necturus* proximal tubule cells (29). However, Na activities of 11–15 meq/liter obtained in isolated perfused *Necturus* proximal tubules (10, 37) appear to be systematically lower than the intracellular Na activity of 21.4 meq/liter measured in the present study. In any case, the intracellular Na activity of

either animal is greatly below the value expected for an equilibrium distribution across either the luminal or basolateral membranes. This clearly indicates active Na transport out of the cell.

The mean intracellular K activity of 54.7 meq/liter for *Ambystoma* proximal tubule is close to the intracellular K activity found in *Necturus* proximal tubules either in vivo—58.7 meq/liter (30)—or doubly perfused—59.6 meq/liter (33)—as well as close to the K activity of 48.6 meq/liter found in rabbit proximal tubules (2). However, it is lower than the value of 67.4 meq/liter reported for bullfrog proximal tubule (17) and the value of 82.6 meq/liter found in rat proximal tubule cells (12). Nonetheless, the intracellular K activity in *Ambystoma* proximal tubule is clearly above the value expected for a purely passive distribution across either cell membrane (51). This is strong evidence for active transport of K into the cell via the basolateral Na-K ATPase. It should be pointed out that all values of intracellular K activity in amphibian proximal tubules are significantly lower than the K activity of 87.3 meq/liter reported for *Necturus* gallbladder epithelium (47).

The mean intracellular Cl activity of 15.3 meq/liter is close to Cl activities previously reported for proximal tubules of *Ambystoma*: 16.8 meq/liter (4); blood-perfused *Necturus*: 15.9 meq/liter (29); and doubly perfused *Necturus*: 13.2 meq/liter (21). However, it is significantly greater than the value of 9.9 meq/liter reported for bullfrog proximal tubule cells (17), but significantly less than the single report of 24.5 meq/liter in doubly perfused *Necturus* (55). In all cases, intracellular Cl is above the value predicted by a purely passive distribution across either cell membrane, which indicates that Cl is accumulated by the cell via some process coupled either directly or indirectly to metabolic energy.

Effect of Bath K Removal

Table II and Fig. 2 summarize the effect on intracellular Na, K, and Cl activities of removal and re-addition of bath K. The bottom tracing in Fig. 2 indicates bath potassium activity as a function of time. Clearly, removal of K from the bath increases intracellular Na and Cl and decreases cell K. The intracellular ionic activities after 20 min of K-free bath are summarized in the second row of Table II. The corresponding control values for this group of tubules are given in the first row of Table II. The observed reciprocal changes in Na and K during the transition from control to zero K most likely result from inhibition of the basolateral Na-K ATPase. The increase in cell Cl by 13.6 meq/liter during removal of bath K roughly balances the net increase in cell cations from 76.1 to 90.3 meq/liter because of the excess of Na influx over K efflux during this period.

Since the effect of bath K removal on ion activities and electrical potentials has been reported previously (51), Table II and Fig. 2 concentrate on the effect of returning K^+ to the bath solution after a 20-min period in K-free bathing solution. Therefore, in Fig. 2 the time scale of intracellular activity changes during removal of bath K has been greatly compressed.

Effect of Elevating Bath K After Incubation in a K-free Bath

As illustrated in Fig. 2, return of high K to the bath (time 0 on the abscissa) produces a simultaneous increase in cell K (dashed line) and a decrease in cell Na (solid line). The relatively small percent decrease in bath Na activity between solutions B and C (Table I) was presumed to have no significant effect on the Na pump. The reciprocal changes in cell Na and K illustrated in Fig. 2 are consistent with reactivation of the Na-K pump by bath K. At the same time the decrease in cell Cl^- activity that occurs during this period suggests a net efflux of Cl from the cell. This Cl efflux is in a direction that compensates for the excess drop in cell Na over the increase in cell K. It should be noted that 5 min after reactivation of the pump, both intracellular K and intracellular Cl activities exceed control levels, whereas cell Na activity is actually below its control value. This results from an accumulation of KCl by the cells, which is to be expected with a 5-min exposure to an elevated K concentration in the bath.

The slope of these ion activity curves in Fig. 2 at times between 0 and 5 min cannot provide exact information about net influxes unless the instantaneous volume-area relationship of the cell is known. For example, proximal tubule cells swollen during inhibition of active transport tend to shrink slightly during re-activation of the Na-K pump. Therefore, calculations based on the slope of the K activity curve in Fig. 2 would overestimate net K influx into the cell, and calculations based on the slope of the Na activity curve in Fig. 2 would underestimate the net Na efflux out of the cell. In view of the difficulty in determining pump fluxes from activity changes, the measured intracellular and extracellular ionic activities were used primarily to calculate the time course of the Nernst equilibrium potentials for each ion across the basolateral membrane. These Nernst potentials can be compared with the measured basolateral membrane potential (V_1) to determine the time interval during which the membrane potential cannot be explained by diffusion processes.

The effect of basolateral potassium removal and re-addition on the measured basolateral (V_1) and transepithelial (V_3) potentials is indicated in Fig. 3 and Table II. The time course of the luminal membrane potential (V_2) shown in Fig. 3 was obtained by subtraction of V_1 from V_3. At time zero, after 20 min of K-free bath, elevation of basal side K hyperpolarizes both the basolateral cell membrane potential (V_1) and the transepithelial potential (V_3), as a consequence of stimulating the basolateral Na-K pump. The low paracellular resistance of the epithelium leads to electrical coupling between the two cell membranes so that the primary basolateral hyperpolarization is reflected as a simultaneous positive change in luminal membrane potential (V_2).

Comparison of the Nernst Equilibrium Potentials with the Observed Basolateral Membrane Potential

Fig. 4 indicates the time course of the Nernst equilibrium potentials for Na, K, and Cl on the same time scale that was used in Figs. 2 and 3. These values

of E_{Na}, E_K, and E_{Cl} were calculated according to Eq. 15 from the intracellular and extracellular ionic activities illustrated in Fig. 2. For comparison, Fig. 4 also indicates the time course of the basolateral membrane potential (V_1).

Under control conditions, E_K is more negative than V_1, and intracellular K is higher than the 24 meq/liter that would be predicted from a purely passive distribution of K across the basolateral membrane. This is consistent with active K transport into the cell by the Na-K ATPase. During the period denoted as K-free, the effective bath K activity was actually ~0.05 meq/liter. Since measurements of bath K activity under nominally K-free conditions are

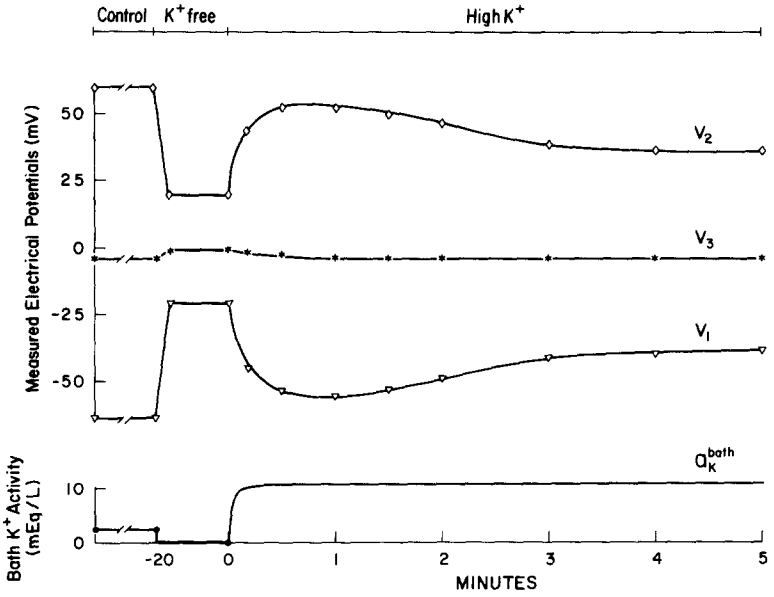

FIGURE 3. The effect of basolateral potassium removal and re-addition (shown in the bottom tracing) on the measured luminal (V_2), basolateral (V_1), and transepithelial (V_3) potential differences. Before time zero, the bath solution was maintained essentially K-free for 20 min. The time course of the electrical potentials during both the control and K-free periods is greatly compressed. At time zero on the abscissa, bath K activity is abruptly increased to 11 meq/liter and maintained at this level.

variable, minimal importance should be attached to the absolute value of E_K during this period. At time zero, elevation of bath K produces a rapid depolarization of the Nernst potential, E_K (upward deflection), even before significant changes in cell K have occurred. At the same time, V_1 rapidly becomes more negative than E_K and remains hyperpolarized relative to E_K for ~3 min (Fig. 4). The peak depolarization of E_K occurs 10 s after reintroduction of bath K. At longer times there is a slow, continuous hyperpolarization of E_K caused by a gradual increase in cell K arising from both active and passive K transport into the cell. Finally, at times >3 min, V_1 becomes slightly more positive than E_K and remains in this depolarized state

relative to its control value because bath K activity is maintained at 11 meq/liter.

On the other hand, under control conditions, E_{Na} is much more positive than V_l, which implies that intracellular Na is normally greatly below the

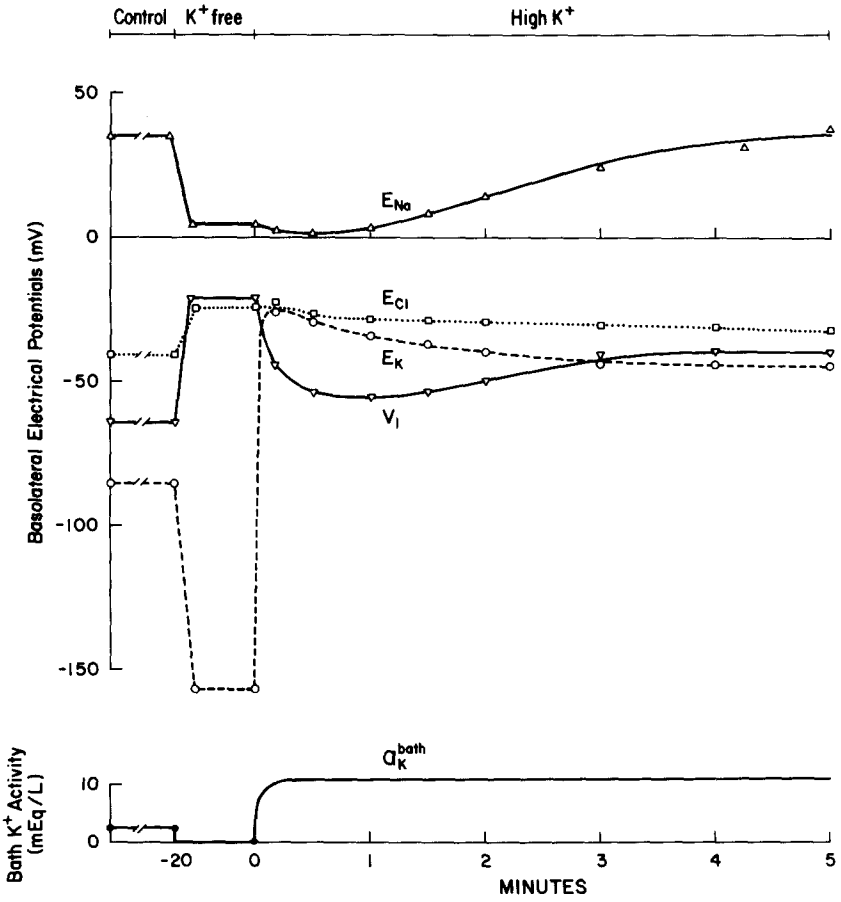

FIGURE 4. The effect of basolateral potassium removal and re-addition (shown in the bottom tracing) on the basolateral electromotive forces for sodium (E_{Na}, solid line), potassium (E_K, dashed line), and chloride (E_{Cl}, dotted line). For comparison, the measured basolateral membrane potential is shown on the same tracing. Before time zero, the bath solution was maintained essentially K-free for 20 min. The time course of the electrical potentials during both the control and K-free periods is greatly compressed. At time zero on the abscissa, bath K activity is abruptly increased to 11 meq/liter and maintained at this level.

value of 94.1 meq/liter that would be predicted for a passive distribution of Na across the basolateral membrane. This is consistent with active extrusion of Na out of the cell by the basolateral Na-K pump. During exposure to K-free bathing solution, intracellular Na reaches a value close to the Na activity

in the extracellular solution. This results in an E_{Na} of only +4.8 mV compared with a control E_{Na} of +34.5 mV. Since return of bath K at time zero is accompanied by an 11 meq/liter decrease in bath Na activity (caused by replacement of Na with K), but only a negligible decrease in cell Na, the basolateral E_{Na} initially decreases from +4.8 to +1.3 mV. At times >1 min after return of bath K, the decrease in intracellular Na at constant extracellular Na activity results in a slow, continuous shift of E_{Na} to more positive values. Under all conditions indicated in Fig. 4, E_{Na} is more positive than V_1.

Under control conditions, E_{Cl} is slightly more positive than V_1, and intracellular Cl is somewhat higher than the value of 6.2 meq/liter that would be expected for a passive distribution of this ion across the basolateral membrane. Furthermore, since extracellular Cl^- activity remains unchanged throughout this experimental protocol, the time course of E_{Cl} is determined exclusively by changes in intracellular Cl activity. The rise in cell Cl that occurs during the period of exposure to a K-free bath depolarizes E_{Cl} from −40.8 to −23.8 mV. During re-activation of the Na-K pump at time zero, there is a small decrease in cell Cl activity. This results in a small, gradual hyperpolarization of E_{Cl} to more negative values. However, the Cl equilibrium potential E_{Cl} is always more positive than V_1, except during removal of K from the bath, when E_{Cl} is approximately equal to V_1.

The measured basolateral membrane potential (V_1) can also be compared to the weighted contribution of the Na, K, and Cl equilibrium potentials. Since under control conditions V_1 is more negative than E_{Na} and E_{Cl}, but less negative than E_K, the basolateral membrane potential could be explained as a sum of ionic diffusion potentials, each weighted by its relative transference number. Consequently, there is no a priori requirement for the pump to be rheogenic under control conditions. During removal of K from the bath, V_1 could be explained either as a Cl equilibrium potential or as a K equilibrium potential diminished by contributions from E_{Na}. At time zero, reactivation of the basolateral Na-K pump by return of bath K almost immediately hyperpolarizes V_1 to a value that is consistently more negative than either E_K, E_{Cl}, or E_{Na}. Furthermore, for almost 3 min, V_1 continues to be more negative than any of the Nernst potentials, which indicates that it cannot be explained as simply a result of ionic diffusion potentials. Since E_{Na} and E_{Cl} are always more positive than E_K (Fig. 4), the algebraic difference between V_1 and E_K at any time after return of bath K represents the minimum rheogenic potential difference directly generated by the Na-K pump. As illustrated in Fig. 4, this minimum rheogenic contribution to the basolateral membrane potential reaches a peak value of −22.2 mV ($= V_1 - E_K$) at ~1 min after the return of K to the bathing solution. However, after ~3 min, the minimum rheogenic contribution to the basolateral potential has effectively declined to zero.

DISCUSSION

Evidence for a Rheogenic Na-K Pump in Epithelia

Although the Koefoed-Johnsen and Ussing (32) model of epithelial Na transport suggested a neutral Na-K pump, subsequent studies have for the

most part indicated an epithelial Na-K pump that is rheogenic, at least under certain experimental conditions. In frog skin, measurements of Na and K fluxes provided evidence of a rheogenic process at the serosal membrane by demonstrating an excess of Na efflux over K influx (1, 3). In both frog skin (9) and toad bladder (14, 23), neither the short-circuit current nor the open-circuit transepithelial potential seem to be strictly determined by the serosal K diffusion potential, as would be predicted by the original Koefoed-Johnsen and Ussing model (32). Furthermore, although paracellular diffusion potentials have been suggested as a source for the transepithelial potential in mammalian gallbladder (38), subsequent experiments have indicated that diffusion potentials across an ion-selective tight junction are insufficient to account for the observed transepithelial potential in gallbladder (19). Thus, these transepithelial measurements constitute indirect evidence for a rheogenic Na-K pump at the serosal membrane of many epithelial tissues.

The results of intracellular potential and ionic activity measurements have generally provided more direct evidence that the Na-K pump of most epithelia operates in a rheogenic manner. In early microelectrode experiments with toad bladder cells, the observed serosal membrane potential was found to exceed the maximum potassium diffusion potential across that membrane (15). In both rabbit gallbladder (19) and rabbit ileum (45), microelectrode experiments have demonstrated serosal membrane potentials that appear to be highly sensitive to cooling and oxygen deprivation. In addition, application of amphotericin B to the mucosal side of mammalian gallbladder resulted in the rapid development of a serosal-positive electrical potential whose magnitude appeared to be relatively independent of cell membrane ionic diffusion potentials (44). Although the results of K elevation, cooling, oxygen deprivation, and amphotericin treatment are consistent with rheogenic Na-K transport, the complicated effects of each of these experimental maneuvers make a simple interpretation extremely difficult. More recent experiments using amiloride-treated frog skins have indicated that ouabain depolarizes the serosal membrane potential before any significant changes in cell electrolyte composition have occurred (41). This constitutes good evidence for a ouabain-sensitive rheogenic Na-K pump at the serosal membrane.

Further evidence for a serosal rheogenic process comes from experiments with mammalian urinary bladder and colon using stepwise elevation of mucosal Na in nystatin-treated preparations (36, 62). Rheogenic Na-K transport was also demonstrated in these tissues under less drastic maneuvers, such as during return of serosal K after a period of incubation in K-free media (61). However, the relatively small predicted contribution of rheogenic Na-K transport to the normal resting potential in urinary bladder and colon makes it difficult to demonstrate that Na-K transport in these tissues is rheogenic under normal, unstimulated conditions. The issue of whether the Na-K pump is rheogenic under normal conditions is still controversial since in *Necturus* gallbladder there is evidence that the Na-K pump at the serosal membrane may sometimes appear to operate in a neutral fashion (46).

Rheogenic Na-K transport has generally been more difficult to demonstrate in renal epithelia than in flat epithelia. Early measurements of both intracellular potentials and chemical composition in Na-loaded renal slices provided evidence that membrane potentials could sometimes exceed ionic diffusion potentials at the basolateral membrane of the proximal tubule (43). However, in renal slices, the absence of transepithelial transport and the multiple cell types in the slice may prevent an accurate comparison between chemically determined electrolyte content and intracellular membrane potential. A further complication has been the postulated existence of two separate active pumps at the basolateral membrane of the proximal tubule: the first extrudes Na from the cell in a rheogenic manner, and the second exchanges Na for K and is ouabain sensitive (60). In doubly perfused *Amphiuma* kidneys, microelectrode experiments have provided some evidence for rheogenic transport at the basolateral membrane of the renal distal tubule.[1]

In isolated perfused proximal tubules, recent determinations of both intracellular potential and K activity favor a Na-K pump that is rheogenic at least under some conditions (2). In these experiments, incubation of tubules in low-K solutions (0.1 mM), followed by elevation of serosal K, resulted in basolateral membrane potentials that were significantly larger than the E_K of that membrane (2). Although this demonstrates a rheogenic Na-K pump, the average basolateral potential of −37.8 mV reported in these studies (2) is about half the basolateral membrane potential reported for either mammalian or amphibian proximal tubules (6, 12).

In the present experiments on salamander proximal tubules, which involved measurement of intracellular Na, Cl, and K activities as well as other electrical parameters, a similar procedure of K removal, followed by the return of higher than normal K to the serosal solution, resulted in basolateral membrane potentials that always exceeded the equilibrium potentials of Na, K, or Cl (Fig. 4 and Table II). This constitutes clear evidence that the basolateral Na-K pump of the proximal tubule is rheogenic, at least under these conditions. Furthermore, this qualitative demonstration of a rheogenic process does not depend on any assumptions about changes in cell volume, permeability coefficients, resistances, or current flow.

However, the data in Fig. 4 alone do not provide conclusive evidence that the renal Na-K pump is rheogenic under all conditions. For example, during the normal unstimulated state, the basolateral membrane potential could be explained largely as a K diffusion potential diminished by contributions from E_{Na} and E_{Cl}. To determine whether the renal Na-K pump is rheogenic under control conditions, it is necessary to compare the observed basolateral membrane potential (V_1) with the potential (E_1) calculated from the constant field equation. Furthermore, actual estimation of the pump current associated with the basolateral active transport system requires some type of equivalent

[1] Wiederholt, M., L. L. Hansen, U. Teuscher, B. Cohen, and G. Giebisch. Relationship between peritubular membrane potential and net fluid reabsorption in the distal renal tubule of *Amphiuma*. Manuscript submitted for publication.

circuit representation for the renal epithelium. These quantitative issues of pump current and pump stoichiometry are addressed in the next section.

Quantitative Determination of Rheogenic Currents

Although most evidence, including the results of experiments described in this paper, favor an epithelial Na-K pump that is rheogenic, there have been relatively few estimates of either the currents or the exact stoichiometry of the intact epithelial Na-K pump. One preparation in which this issue has been recently examined is the rabbit urinary bladder, where the rheogenic Na-K pump current is calculated as the difference between total membrane current and the current attributable to diffusion processes (35). Comparison of this pump current with estimates of net Na transport by the pump has yielded Na/K coupling ratios in the neighborhood of 3:2 (35). A similar stoichiometry has also been obtained in the same preparation from the observed dependence of rheogenic pump current on the intracellular Na and serosal K, assuming a model of highly cooperative binding (35).

In the turtle colon, comparison of the amphotericin-induced increment in Na absorption and K secretion has indicated a Na/K coupling ratio of ~3:2 for the serosal membrane Na-K pump (31). In frog skins, rheogenic Na-K pump current has been measured as the short-circuit current immediately after blockage of the serosal K channels with barium (42). Comparison of this pump current with net Na transport (equal to normal short-circuit current) has indicated a stoichiometry of $3Na^+$ to $2K^+$ for the frog skin Na-K pump.

In the present experiments the data illustrated in Figs. 2–4 permit determination of the current generated by the renal Na-K pump if the tubular epithelium is represented by the electrical equivalent circuit of Fig. 5. Since this circuit has been discussed extensively (5, 7, 51), only the main features of the model are presented below.

The Electrical Equivalent Circuit

The dashed lines in Fig. 5 indicate the cell boundaries of the renal proximal tubule epithelium. The measured basolateral, luminal, and transepithelial potential differences are denoted respectively by V_1, V_2, and V_3, and the total ionic diffusion potentials across the basolateral and luminal cell membranes are denoted respectively by E_1 and E_2. The term E_3 represents the paracellular emf resulting from a combination of dissipative processes across the tight junction and across the basal end of the paracellular space. Even with identical solutions in lumen and bath, E_3 may be different from zero because of slight differences between the ionic composition of the lumen and the paracellular space. The basolateral, luminal, and paracellular electrical resistances are denoted respectively by R_1, R_2, and R_3 and are expressed in units of ohms times square centimeter of epithelium. Finally, the current source (i_1^a) is defined as the current arising from an active basolateral rheogenic process.

The actual values of the cell membrane emf's are calculated from the constant field equation using measured intracellular and extracellular ionic

activities. For example, the emf across the basolateral cell membrane is given by:

$$E_1 = -\frac{RT}{F} \ln \frac{a_K^{cell} + [P_{Na}/P_K]\, a_{Na}^{cell} + [P_{Cl}/P_K]\, a_{Cl}^{bath}}{a_K^{bath} + [P_{Na}/P_K]\, a_{Na}^{bath} + [P_{Cl}/P_K]\, a_{Cl}^{cell}}. \quad (16)$$

Estimates of the basolateral permeability ratios, $P_{Na}/P_K = 0.03$ and $P_{Cl}/P_K = 0.2$, were obtained in separate experiments in our laboratory during rapid alterations of bath Na, K, and Cl composition. The alterations in K activity were carried out with bath K activities >10 meq/liter in order to minimize

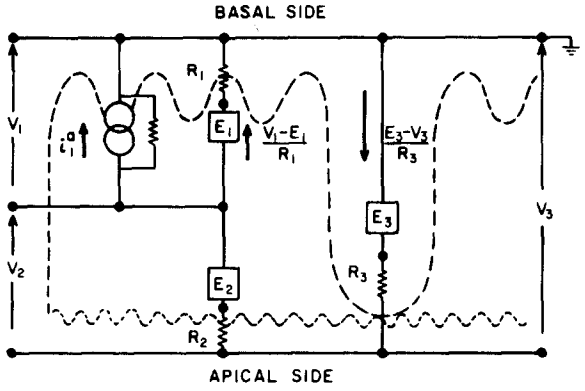

FIGURE 5. The electrical equivalent circuit used to represent the renal proximal tubule epithelium. The dashed lines indicate the cell borders. V_1, V_2, and V_3 are the measured basolateral, luminal, and transepithelial potential differences, respectively. E_1 and E_2 are the total ionic electromotive forces across basolateral and luminal cell membranes calculated from intracellular and extracellular ionic activities. E_3 is the paracellular electromotive force resulting from a combination of dissipative processes across the tight junction and across the basal end of the paracellular space. R_1, R_2, and R_3 are the basolateral, luminal, and paracellular electrical resistances. The current source (i_1^a) is defined as the current arising from an active basolateral rheogenic process.

the effect of changes in K on the activity of the Na-K pump. Obviously, this type of permeability measurement cannot be performed during any experimental procedure that investigates the dependence of Na-K ATPase activity on external K. Hence, the ionic permeability ratios obtained under control conditions were assumed to apply throughout the experimental protocol. Using these permeability ratios and the measured intracellular and extracellular ionic activities, the calculated control value of E_1 was −57.9 mV, which can be compared with an average basolateral membrane potential (V_1) of −64 mV and an average control E_K of −85.4 mV.

Although transepithelial resistance could be measured throughout the experimental protocol, reliable determinations of the cell membrane resistances (R_1 and R_2) were obtained only during control conditions using the procedure outlined in the Methods section. Consequently, the value of R_1 at

different bath K activities had to be estimated from Eq. 17, which describes the effect of ionic activities on the cell membrane resistance (assuming constant permeability ratios):

$$R_1 = R_1^o \frac{(K)_b^o + [P_{Na}/P_K](Na)_b^o + [P_{Cl}/P_K](Cl)_c^o}{(K)_b + [P_{Na}/P_K](Na)_b + [P_{Cl}/P_K](Cl)_c} \cdot \frac{E_1^o}{E_1} \cdot \frac{1 - \exp(E_1F/RT)}{1 - \exp(E_1^oF/RT)}. \quad (17)$$

Eq. 17 was adapted from the expression for total membrane conductance derived in the appendix of reference 24. In Eq. 17, the term R_1^o denotes the value of basolateral membrane resistance measured under control conditions and listed in Table III. The terms (K), (Na), and (Cl) denote respectively the K, Na, and Cl activities. The subscripts b and c indicate bath and cell, and the superscript o denotes the control value of the parameter.

As indicated in Table III, the average control value of basolateral cell membrane resistance was $R_1^o = 591.6\ \Omega cm^2$. Using the values of R_1 calculated from Eq. 17 and measurements of R_{te} and α, the paracellular resistance (R_3) can be determined at any time according to Eq. 6. Since the paracellular pathway in the renal proximal tubule has a much lower resistance than the transcellular pathway, the measured transepithelial resistance is approximately equivalent to the paracellular resistance, R_3. For example, in Table III the value of R_3 is $65.5\ \Omega cm^2$, as compared with a transepithelial resistance of $R_{te} = 63.6\ \Omega cm^2$. In general, the value of R_3 is ~2% larger than the transepithelial resistance of the salamander proximal tubule. Although the apical membrane resistance, R_2, is not required for the calculation of rheogenic currents, its value can be estimated from R_1 and α, the ratio of apical to basolateral voltage deflections during a lumen-to-bath injection of current (7).

The actual value of basolateral rheogenic current is obtained by applying Kirchoff's current law to the circuit of Fig. 5. Specifically, i_1^a is calculated as the algebraic difference between the total current through the paracellular path, $(E_3 - V_3)/R_3$, and the total current through all basolateral membrane ionic conductances, $(V_1 - E_1)/R_1$. Namely,

$$i_1^a = (E_3 - V_3)/R_3 - (V_1 - E_1)/R_1. \quad (18)$$

Although there is some evidence that the renal Na-K ATPase functions as a constant current source, computation of the value of i_1^a does not strictly depend on a current source representation.

Calculation of Rheogenic Currents

The rheogenic current (i_1^a) was calculated from Eq. 18 using the continuously measured values of basolateral (V_1) and transepithelial potential (V_3). The basolateral emf (E_1) was calculated from Eq. 16 using the control permeability ratios and the continuously measured ionic activities. The basolateral cell membrane resistance (R_1) was calculated from Eq. 17 using the continuously measured ionic activities and the control values given in Table III. Finally, paracellular resistance (R_3) was determined from Eq. 6 using the calculated value of R_1 together with the measured values of α and R_{te}. In

these experiments the paracellular emf (E_3) could be neither measured nor derived from measured parameters. Consequently, rheogenic currents were calculated for a range of possible E_3 values.

Fig. 6 illustrates the effect of basolateral K removal and re-addition (bottom tracing) on the total basolateral emf (E_1) and the basolateral rheogenic current

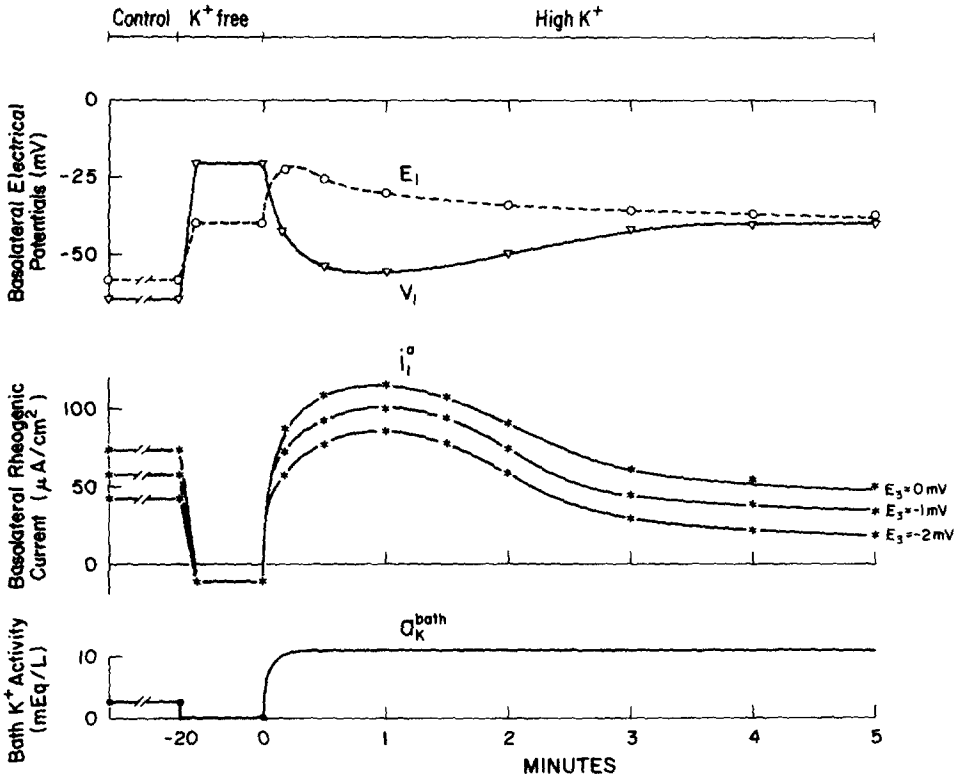

FIGURE 6. The effect of basolateral potassium removal and re-addition (shown in the bottom tracing) on the total basolateral electromotive force, E_1 (top panel) and the basolateral rheogenic current, i_1^a (middle panel). For comparison, the measured basolateral membrane potential, V_1, is shown in the top panel on the same time scale. Before time zero, the bath solution was maintained essentially K-free for 20 min. The time course of the electrical potentials and rheogenic current during both the control and K-free periods is greatly compressed. At time zero on the abscissa, bath K activity is abruptly increased to 11 meq/liter and maintained at this level. As indicated in the middle panel, the absolute magnitude of the calculated basolateral rheogenic current is dependent on the assumed value of the paracellular emf, E_3.

(i_1^a), where E_1 was calculated from Eq. 16 and i_1^a was calculated from Eq. 18. Under control conditions, V_1 is 6 mV more negative than the calculated basolateral emf, E_1, which indicates that ionic diffusional processes can account for almost 90% of the observed basolateral potential (V_1) during

normal conditions. The remaining 10% of the basolateral membrane potential appears to arise from a rheogenic process.

As illustrated in the middle section of Fig. 6, the calculated rheogenic current, i_1^a, depends strongly on the assumed value of the paracellular diffusion potential E_3. Even though the use of identical lumen and bath solutions during control conditions prevents development of large paracellular diffusion potentials, E_3 may not be exactly zero since interspace NaCl concentration in a transporting proximal tubule is significantly above the luminal NaCl concentration and probably above the bath NaCl concentration as well. Therefore, any difference between the ionic selectivity properties of the tight junction and the basal end of the interspace will lead to a non-zero value of E_3. Since the salt concentration of the paracellular space cannot be measured directly and can be estimated only under control conditions, there is no real way to determine the value of E_3 during removal and re-addition of bath K. However, the strong anion selectivity of the tight junction in the proximal tubule of amphibia suggests a paracellular emf (E_3) in the range -2 mV $\leq E_3 \leq 0$ mV (5, 49, 51).

During the period of bath K removal, transepithelial Na and water reabsorption are blocked. This would presumably be associated with the dissipation of all ionic gradients between the paracellular space and the lumen or bath solutions. Hence, E_3 should be zero during this period. Removal of bath K is also associated with a depolarization of the transepithelial potential (V_3) to a value of -1 mV and a depolarization of the basolateral potential (V_1) to a value that is less negative than the calculated basolateral emf (E_1). This actually results in a slightly negative value of a basolateral rheogenic current, i_1^a, which may not be significantly different from zero when one considers the assumptions involved in the calculations.

As shown in Fig. 6, return of higher than normal K to the bath elevates the pump current i_1^a to a broad peak that attains a relative maximum at about $t = 1$ min. The appearance of a maximum in both i_1^a and V_1 almost 1 min after bath K reaches 11 meq/liter suggests a substantial diffusion delay between the well-stirred bathing solution and the active pump sites located on infoldings of the basolateral membrane. As with the control state, the height of the i_1^a curve is strongly determined by the value of E_3.

At times >1 min after return of bath K, there is a parallel decline of both pump current and basolateral membrane potential. Since both E_K and E_{Cl} hyperpolarize during this period, the calculated value of E_1 would never depolarize even if the return of bath K increased basolateral K or Cl conductance. Hence, at times >1 min after return of K to the bath, V_1 cannot be explained solely on the basis of a diffusion process. For this reason it seems likely that the change in V_1 is a consequence of the decrease in positive, basolateral pump current that occurs during this time.

Dependence on Intracellular Sodium

At times >1 min after return of bath K, the decrease in pump current (i_1) is associated with changes in both membrane potential and intracellular ionic

composition. However, it is unlikely that the depolarization of membrane potential causes the decrease in i_l^a since positive-going changes in V_1 would be expected to increase rather than decrease the outward, positive pump current. It is also unlikely that either increases in cell K in the range observed or small decreases in cell Cl are responsible for the decline in i_l^a (25).

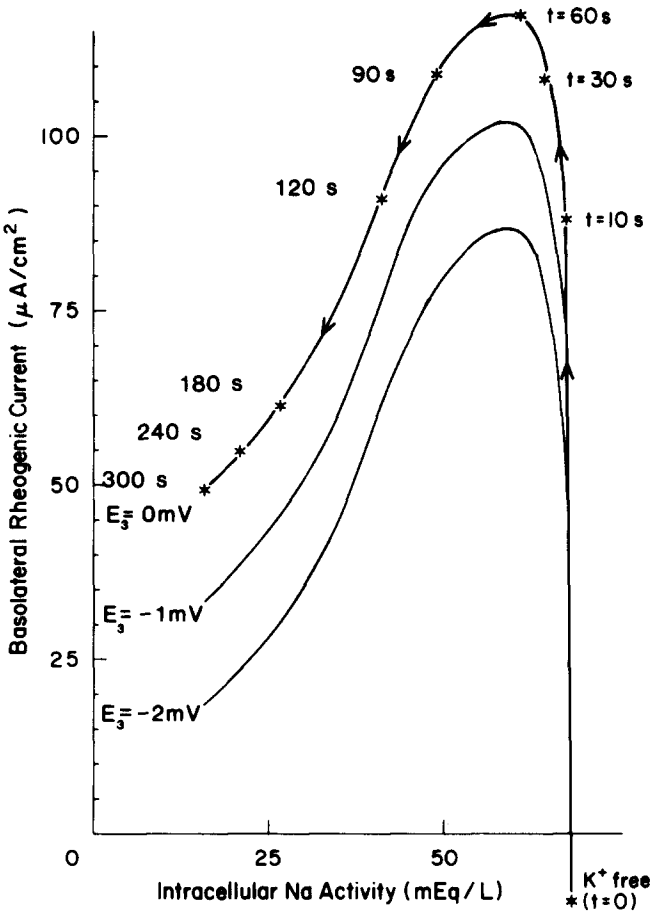

FIGURE 7. Dependence of basolateral rheogenic current, i_l^a, on intracellular sodium activity during recovery from a potassium-free bath (serosal) solution. After a 20-min incubation in potassium-free bathing solution, elevation of bath K rapidly stimulates the basolateral rheogenic current, which reaches a maximum at 60 s after the start of potassium addition to the bath. At times >60 s, basolateral rheogenic current is directly proportional to intracellular sodium activity. As indicated, the absolute magnitude of the calculated basolateral rheogenic current is dependent on the assumed value of E_3.

Therefore, the decrease in intracellular Na is most likely responsible for the decline in i_l^a at times >1 min. This would be consistent with results of biochemical studies on the Na dependence of isolated Na-K ATPase (25). Further details on the relationship between basolateral rheogenic current

and intracellular Na are illustrated in Fig. 7. All values of t in Fig. 7 indicate the time elapsed since the transition from a K-free bath to a bath solution having a K^+ activity of 11 meq/liter.

At times <60 s, there is a steep increase in basolateral rheogenic current i_1^a, which actually occurs concomitantly with a slight decrease in cell Na. This may indicate that when K is returned to the bath, the pumps most accessible to the bathing solution begin to transport Na out of the cell before the less accessible pumps are reactivated.

At times >60 s, there is a progressive decline in basolateral rheogenic current which is paralleled by a decrease in intracellular Na activity. The actual magnitude of the decline in i_1^a depends on the assumed value of the paracellular emf (E_3) during this period. The more negative the value of E_3, the lower the absolute magnitude of the basolateral rheogenic currents. If the source of the rheogenic current (i_1^a) is indeed the basolateral Na-K ATPase, one would expect i_1^a to approach zero as intracellular Na approaches zero. This assumption would tend to favor the curve in Fig. 7 that corresponds to $E_3 = -2$ mV. However, since intracellular Na activity never spontaneously declined below 16 meq/liter in these experiments, it is possible that i_1^a drops off precipitously at low intracellular Na activities. This might cause any of the three curves to pass through the origin. Regardless of the exact functional dependence of i_1^a on intracellular Na, it seems clear that at times >1 min the decrease in rheogenic pump current correlates with the decrease in intracellular Na activity.

Stoichiometry of the Renal Na-K Pump

Although the rheogenic currents associated with the Na-K pump can be calculated from Eq. 18, determination of the pump stoichiometry depends on an independent measure of either the Na or the K current carried by the pump. If i_{Na}^a represents the outward Na pump current and i_K^a represents the inward K pump current, the net pump current i_1^a is equal to $i_{Na}^a - i_K^a$, and the coupling ratio of the pump (r) is defined by:

$$r = i_{Na}^a / i_K^a. \tag{19}$$

Similar expressions can be written for r in terms of i_1^a and either the K pump current i_K^a or the Na pump current i_{Na}^a:

$$r = 1 + (i_1^a / i_K^a); \tag{20}$$

$$r = 1/(1 - i_1^a / i_{Na}^a). \tag{21}$$

Use of Eq. 19 requires estimates for both i_{Na}^a and i_K^a, whereas Eqs. 20 and 21 require estimates of either i_{Na}^a or i_K^a. Unfortunately, precise values of these ionic currents cannot be calculated from the instantaneous slope of the ionic activity curves in Fig. 2 for two reasons. First, Na and K transport also occurs by routes other than via the basolateral Na-K pump, and second, cell volume changes can produce alterations in ionic activity that do not reflect net ion transport (54). Nonetheless, it is possible to use the observed alterations in intracellular Na and K activity to calculate a minimum value of the pump Na current and a maximum value of the pump K current.

At any time after the return of K to the bath ($t > 0$), the lower limit on the pump Na current i^a_{Na} is related to the rate of decrease of cell Na activity ($-da^{cell}_{Na}/dt$) according to:

$$i^a_{Na} \geq F(V/A)(1/\gamma^{cell}_{Na})(-da^{cell}_{Na}/dt), \quad (22)$$

where F denotes the Faraday constant and γ^{cell}_{Na} is the intracellular Na activity coefficient estimated as 0.48 from reference 28. As indicated by Eq. 22, the rate of decrease of cell Na activity underestimates the Na pump current for $t > 0$ both because of continual entry of Na across the luminal membrane and because of a slight decrease in cell volume that occurs during the return of bath K. The volume-to-area ratio (V/A) appearing in Eq. 22 is the product of cell volume per millimeter of tubule and millimeter of tubule per square

TABLE IV

Limits on the Na/K Coupling Ratio of the Na-K Pump During the Period of Pump Reactivation

Time	i^a_t	da^{cell}_{Na}/dt	da^{cell}_{K}/dt	Volume / Area	γ_{Na}	γ_K	i^a_{Na}	i^a_K	Coupling ratios calculated by methods: I	II	III
min	*μA/cm²*	*meq/liter/min*	*meq/liter/min*	*10⁻⁴ cm*			*μA/cm²*	*μA/cm²*			
1	116.8	−17.5	13.0	25.4	0.48	0.58	>148.9	<91.6	>1.6	>2.3	<4.6
1.5	109.6	−20.0	11.0	25.4	0.48	0.58	>170.2	<77.5	>2.2	>2.4	<2.8
2	91.0	−16.1	9.1	25.4	0.48	0.58	>137.0	<64.1	>2.1	>2.4	<3.0
3	61.1	−10.2	4.5	25.4	0.48	0.58	>86.8	<31.7	>2.7	>2.9	<3.4

Time denotes the time after elevation of bath K activity from 0.05 meq/liter (zero-K solution) to 11 meq/liter. da^{cell}_K/dt and da^{cell}_{Na}/dt are the instantaneous slopes calculated from the activity curves in Fig. 2. The volume/area ratio is obtained from reference 39, as described in the text. γ_{Na} and γ_K are the intracellular activity coefficients for Na and K obtained from references 17, 29, and 30. i^a_{Na} and i^a_K are the pump Na and K currents as calculated from Eqs. 22 and 23. Limits on the Na-to-K coupling ratio were calculated from Eq. 19, method I; Eq. 20, method II; Eq. 21, method III. All calculations in this table assume a paracellular emf equal to zero.

centimeter of epithelium. Since the electrical resistances R_1, R_2, and R_3 are in units of ohms times square centimeter of luminal epithelial surface, self-consistency requires that the unit of square centimeter epithelium used in the volume-to-area ratio be square centimeter of luminal epithelial surface. Ultrastructural studies of *Ambystoma* proximal tubules indicate an average cell volume per millimeter of tubule of 4.77×10^6 μm^3/mm and a mean luminal surface area per millimeter of tubule (excluding microvilli) of 0.188×10^6 μm^2/mm tubule (39). Hence, the calculated average volume-to-area ratio for *Ambystoma* proximal tubules is: $(4.77 \times 10^6$ μm^3/mm$)/(0.188 \times 10^6$ μm^2/mm$) = 25.4$ μm. Using Eq. 22, minimum estimates of Na pump current were calculated at four times after return of bath K. These are listed in the i^a_{Na} column of Table IV.

Similarly, at any time after return of K to the bath, the upper limit on the pump K current i^a_K is related to the rate of increase of cell K activity (da^{cell}_K/dt) according to:

$$i_K^a \leq F(V/A)(1/\gamma_K^{cell})(da_K^{cell}/dt). \quad (23)$$

The terms F and the V/A factor are the same as that in Eq. 22, which was used to calculate the pump Na current. The intracellular K activity coefficient, γ_K^{cell}, is equal to 0.57 (17, 30). As indicated by Eq. 23, the rate of increase of cell K activity overestimates the K pump current for $t > 0$ both because of cell shrinkage and because of a sizable passive K influx across the basolateral membrane since V_1 is appreciably more negative than E_K. Maximum estimates of the K pump current were calculated at four times after return of bath K. These are listed in the i_K^a column of Table IV.

Using these estimates of i_{Na}^a and i_K^a, together with calculated values of i_1^a, Eqs. 19–21 define three separate methods for estimating the Na/K coupling ratio of the pump (r). In the first method, the value of r at any time is estimated as the ratio of the Na pump current i_{Na}^a to the K pump current i_K^a. Since the currents in the i_{Na}^a column of Table IV are underestimates of i_{Na}^a and the currents in column i_K^a of Table IV are overestimates of i_K^a, their ratio (i_{Na}^a/i_K^a) at any time constitutes a minimum estimate of the coupling ratio. Four of these minimum coupling ratio estimates, corresponding to different times after return of bath K, are indicated in the last column of Table IV under method I.

The second method of calculating the coupling ratio of the pump involves the use of Eq. 20, together with values of i_1^a and estimates of the pump K current. Since the values of K pump current in the i_K^a column of Table IV are always overestimates of i_K^a, the value of r calculated from i_1^a and i_K^a using Eq. 20 also represents a minimum estimate of the pump coupling ratio. These coupling ratios (r) are listed in the last column of Table IV under method II for four representative times during the period of pump reactivation. Although Table IV assumes a constant volume-to-area ratio between 1 and 3 min, cell shrinkage during this period would decrease the volume-to-area ratio and thereby could increase with time the minimum estimate of r calculated by method II.

The third method of calculating the coupling ratio of the pump involves the use of Eq. 21 in conjunction with values of i_1^a and estimates of the pump Na current. Since the values of Na pump current in the i_{Na}^a column of Table IV always underestimate the Na pump current, the value of r calculated from i_1^a and i_{Na}^a using Eq. 21 represents a maximum estimate of the pump coupling ratio. This arises because at any given value of i_1^a, the coupling ratio defined by Eq. 21 is always a monotonic decreasing function of i_{Na}^a. Consequently, the underestimates of i_{Na}^a result in overestimates of the coupling ratio. These are calculated at four representative times during the period of pump reactivation under method III in the last column of Table IV.

It should be noted with regard to Table IV that coupling ratios are indicated only for the period between 1 and 3 min after the start of reactivation of the pump. Coupling ratios calculated before 1 min or after 3 min are subject to several major sources of error. First, since the basolateral membrane potential (V_1) does not reach a peak until 1 min after the return of bath K, up to 1 min may be required for K to diffuse into the basal

labyrinth and lateral intracellular space to reactivate pumps along the basolateral cell membrane. If this were the case, the rapid increase in cell K activity at times before 1 min might largely reflect passive rather than active movement of K into the cell. Hence, for $t < 1$ min, calculations based on the slopes of the activity curves in Fig. 2 will greatly overestimate i_K^a and greatly underestimate i_{Na}^a, yielding very small (and meaningless) lower limits for the coupling ratio. Second, the abrupt decrease in cell Cl activity during the first minute after return of K to the bath suggests that most of the cell shrinkage that results from pump reactivation probably occurs at this time. Pump currents calculated during this period of volume change will result in lower

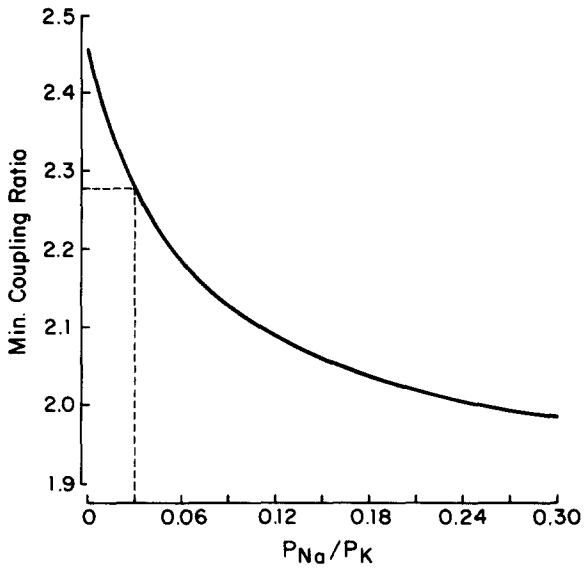

FIGURE 8. The effect of changes in the basolateral membrane relative Na-to-K permeability on the calculated coupling ratio of the Na-K pump. The Cl-to-K permeability ratio was held constant at its control value of 0.2. The minimum coupling ratio was calculated according to Eq. 20 for the time corresponding to 1 min after return of bath K, following incubation in a K-free bathing solution. The paracellular emf was assumed to be negligible. The rectangle indicates a coupling ratio of 2.28, which corresponds to the normal value of P_{Na}/P_K equal to 0.03.

underestimates of i_{Na}^a and higher overestimates of i_K^a than at later times. This will generally lead to a wider range of possible coupling ratios and consequently to a reduction in the usefulness of the technique. Third, the response of the Na-selective electrode may lag behind the response of the fast-acting K-selective electrode by as much as 10 s, depending on the geometry and resistance of the Na electrode. A slow-reacting Na electrode could shift the Na activity curve of Fig. 2 by as much as 10 s to the left. This would steepen the slope of the Na activity curve for any time point before $t = 1.5$ min (the inflection point of the Na activity curve), but the most pronounced effect on

the slope would occur at early times after return of bath K. Hence, at times before $t = 1$ min, method I could predict a coupling ratio of 1.5, which is consistent with the active countertransport of 3Na and 2K. At times >1.5 min, a delay in the Na electrode would result in a slight overestimate of i^3_{Na}, which at most would lower the minimum coupling ratio calculated by method I at $t = 3$ min to 2.1. However, at times >3 min, the effect of a delay in the response of the Na electrode would be more pronounced, which would result in a wide range of permissible coupling ratios. Furthermore, at times >3 min after reactivation of the pump, where the slopes of the Na and K activity

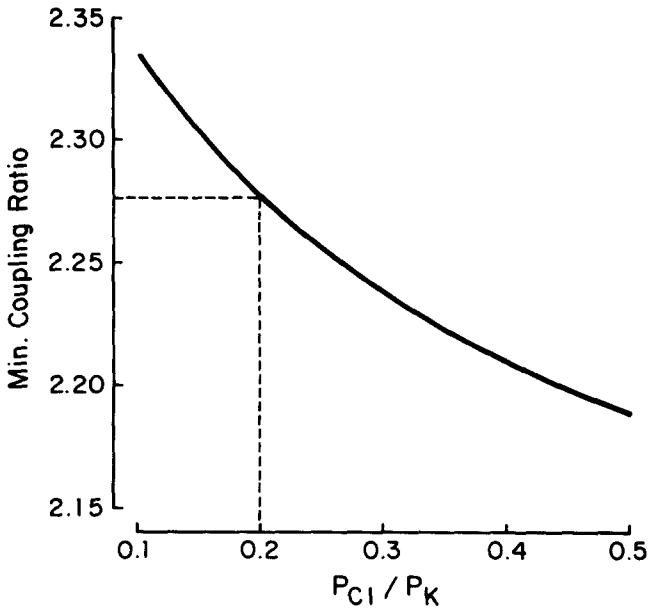

FIGURE 9. The effect of changes in the basolateral membrane relative Cl-to-K permeability on the calculated coupling ratio of the Na-K pump. The Na-to-K permeability was held constant at its control value of 0.03. The minimum coupling ratio was calculated according to Eq. 20 for the time corresponding to 1 min after return of bath K, following incubation in a K-free bathing solution. The paracellular emf was assumed to be negligible. The rectangle indicates a coupling ratio of 2.28, which corresponds to the normal value of P_{Cl}/P_K equal to 0.2.

curves in Fig. 2 become flatter, small errors in determination of these slopes would result in large errors in the calculated coupling ratios.

As Table IV indicates, there is a close similarity in the coupling ratios calculated by methods I and II despite the fact that method I is independent of the circuit in Fig. 5, whereas method II relies heavily on values of the equivalent circuit parameters. In this respect, it is interesting that both methods I and II predict minimum coupling ratios in excess of 1.5 at times between 1 and 3 min after reactivation of the Na-K pump.

A final source of error in the coupling ratio calculations is possible changes

in membrane ionic selectivities that may occur during the procedure of bath K removal and re-addition. As discussed in the Methods section, cell membrane permeability ratios could not be measured during the transition from low to normal bath K. Therefore, the effect of possible changes in ionic permeabilities on the pump coupling ratio was examined analytically.

The effects of varying the basolateral membrane Na/K or Cl/K permeability ratios are illustrated in Figs. 8 and 9. All calculations apply at 1 min after return of bath K. In both figures, the ordinate displays the minimum pump coupling ratio calculated from Eq. 20 according to method II. Calculations were based on method II because method I (Eq. 19) is independent of ionic permeabilities and method III provides information only about the upper limit of the pump coupling ratio.

As illustrated in Fig. 8, an increase in the basolateral P_{Na}/P_K ratio from a control value of 0.03 to a value as high as 0.3 only reduced the minimum coupling ratio from ~2.3 to ~2.0. As indicated in Fig. 9, the pump coupling ratio is even less sensitive to the basolateral Cl-to-K permeability ratio. For example, the basolateral P_{Cl}/P_K ratio would have to increase above 0.5 before the minimum coupling ratio would decrease much below 2.2. Such large changes in the relative ionic permeabilities of the cell membrane are extremely unlikely.

In summary, the values of Table IV as well as Figs. 8 and 9 suggest that during periods of enhanced pump activity the Na-to-K coupling ratio may transiently exceed the value of 3:2 that is normally associated with the plasma membrane Na-K ATPase (20, 25).

The authors gratefully acknowledge the assistance of Dr. Walter Boron in some of the experiments with ion-selective microelectrodes.

This work was supported by Public Health Service Research Grant R01-AM-13844 and Program Project AM-17433 from the National Institute of Arthritis, Diabetes, Digestive and Kidney Diseases. H. Sackin was supported in part by grants R01-AM-29775 and K04-AM-00969 from the National Institute of Arthritis, Diabetes, Digestive and Kidney Diseases. Part of this project was funded by an award from the Biomedical Research Support Grant Program, Division of Research Resources, NIH grant BRSG S07 RR 05396.

A preliminary report of this research was presented at the 11th Annual Meeting of the American Society of Nephrology, New Orleans, LA, 1978, and the 12th Annual Meeting of the Society of Nephrology, Boston, MA, 1979.

Received for publication 28 February 1983.

REFERENCES

1. Aceves, J. 1977. Pumped movements of sodium and potassium ions in the isolated epithelium of frog skin. *Pflügers Arch. Eur. J. Physiol.* 371:201–209.
2. Biagi, B., M. Sohtell, and G. Giebisch. 1981. Intracellular potassium activity in the rabbit proximal straight tubule. *Am. J. Physiol.* 241:F677–F686.
3. Biber, T., J. Aceves, and L. J. Mandel. 1972. Potassium uptake across serosal surface of isolated frog skin epithelium. *Am. J. Physiol.* 222:1366–1373.
4. Boron, W. F., and E. L. Boulpaep. 1983. Intracellular pH regulation in the renal proximal tubule of the salamander: Na-H exchange. *J. Gen. Physiol.* 81:29–52.
5. Boulpaep, E. L. 1976. Electrical phenomena in the nephron. *Kidney Int.* 9:88–102.

6. Boulpaep, E. L. 1979. Electrophysiology of the kidney. *In* Membrane Transport in Biology. G. Giebisch, D. C. Tosteson, and H. H. Ussing, editors. Springer-Verlag, New York. 97–144.
7. Boulpaep, E. L., and H. Sackin. 1979. Equivalent electrical circuit analysis and rheogenic pumps in epithelia. *Fed. Proc.* 38:2030–2036.
8. Boulpaep, E. L., and H. Sackin. 1980. Electrical analysis of intraepithelial barriers. *Curr. Top. Membr. Transp.* 13:169–197.
9. Bricker, N. S., T. Biber, and H. H. Ussing. 1963. Exposure of the isolated frog skin to high potassium concentrations at the internal surface. I. Bioelectric phenomena and sodium transport. *J. Clin. Invest.* 42:88–99.
10. Cemerikic, D., and G. Giebisch. 1981. Intracellular Na activity measurements in *Necturus* kidney proximal tubule. *8th Int. Congr. Nephrology.* 71. (Abstr.)
11. De Weer, P. 1975. Aspects of the recovery processes in nerve. *In* M. T. P. International Review of Science Physiology: Neurophysiology. C. C. Hunt, editor. University Park Press, Baltimore, MD. 3:231–278.
12. Edelman, A., S. Curci, I. Samarzija, and E. Frömter. 1978. Determination of intracellular K activity in rat kidney proximal tubular cells. *Pflügers Arch. Eur. J. Physiol.* 378:37–45.
13. Farquhar, M. G., and G. E. Palade. 1964. Functional organization of amphibian skin. *Proc. Natl. Acad. Sci. USA.* 51:569–577.
14. Finn, A. L. 1974. Transepithelial potential difference in toad urinary bladder is not due to ionic diffusion. *Nature (Lond.).* 250:495–496.
15. Frazier, H. S., and A. Leaf. 1963. The electrical characteristics of active sodium transport in the toad bladder. *J. Gen. Physiol.* 46:491–503.
16. Fujimoto, M., and T. Kubota. 1976. Physicochemical properties of a liquid ion exchanger microelectrode and its application to biological fluids. *Jpn. J. Physiol.* 26:631–650.
17. Fujimoto, M., T. Kubota, and K. Kotera. 1977. Electrochemical profile of K and Cl across the proximal tubule of bullfrog kidneys. (A study of double-barreled ion-sensitive microelectrodes.) *In* Contributions to Nephrology. S. Karger, Basel. 6:114–123.
18. Gadsby, D. C., and P. F. Cranefield. 1979. Electrogenic sodium extrusion in cardiac purkinje fibers. *J. Gen. Physiol.* 73:819–837.
19. Gelarden, R. T., and R. C. Rose. 1974. Electrical properties and diffusion potentials in the gall bladder of man, monkey, dog, goose and rabbit. *J. Membr. Biol.* 19:37–54.
20. Glynn, I. M., and S. J. D. Karlish. 1965. The sodium pump. *Annu. Rev. Physiol.* 37:13–55.
21. Guggino, W. B., E. L. Boulpaep, and G. Giebisch. 1982. Electrical properties of chloride transport across the *Necturus* proximal tubule. *J. Membr. Biol.* 65:185–196.
22. Guggino, W. B., E. E. Windhager, E. L. Boulpaep, and G. Giebisch. 1982. Cellular and paracellular resistances of the *Necturus* proximal tubule. *J. Membr. Biol.* 67:143–154.
23. Herrera, F. 1968. Action of ouabain on bioelectric properties and ion content in toad urinary bladder. *Am. J. Physiol.* 215:183–189.
24. Hodgkin, A. L., and B. Katz. 1949. The effect of sodium ions on the electrical activity of the giant axon of the squid. *J. Physiol. (Lond.).* 108:37–77.
25. Jorgensen, P. L. 1980. Sodium and potassium ion pump in kidney tubules. *Physiol. Rev.* 60:864–917.
26. Kernan, R. P. 1962. Membrane potential changes during sodium transport in frog sartorius muscle. *Nature (Lond.).* 193:986–987.
27. Keynes, R. D., and R. J. Rybova. 1963. The coupling between sodium and potassium fluxes in frog sartorius muscle. *J. Physiol. (Lond.).* 168:58P. (Abstr.)

28. Khuri, R. N. 1979. Electrochemistry of the nephron. *In* Membrane Transport in Biology. G. Giebisch, D. C. Tosteson, and H. H. Ussing, editors. Springer-Verlag, New York. IVA:47–95.

29. Khuri, R. N., S. K. Agulian, E. L. Boulpaep, W. Simon, and G. Giebisch. 1978. Changes in the intracellular electrochemical potential of Na^+, K^+ and Cl^- in single cells of the proximal tubule of the *Necturus* kidney induced by rapid changes in the extracellular perfusion fluid. *Arzneim.-Forsch./Drug Res.* 28:879. (Abstr.)

30. Khuri, R., J. J. Hajjar, S. Agulian, K. Bogharian, A. Kalloghlian, and H. Bizri. 1972. Intracellular potassium in cells of the proximal tubule of *Necturus maculosus*. *Pflügers Arch. Eur. J. Physiol.* 338:73–80.

31. Kirk, K. L., D. R. Halm, and D. C. Dawson. 1980. Active sodium transport by turtle colon via an electrogenic Na-K exchange pump. *Nature (Lond.).* 287:237–239.

32. Koefoed-Johnsen, V., and H. Ussing. 1958. The nature of the frog skin potential. *Acta Physiol. Scand.* 42:298–308.

33. Kubota, T., B. Biagi, and G. Giebisch. 1983. Intracellular K^+ activity measurements in single proximal tubules of *Necturus* kidney. *J. Membr. Biol.* 73:51–60.

34. Kyte, J. 1976. Immunoferritin determination of the distribution of (Na and K) ATPase over the plasma membranes of renal convoluted tubules. II. Proximal segment. *J. Cell Biol.* 68:304–318.

35. Lewis, S. A., and N. K. Wills. 1981. Interaction between apical and basolateral membranes during sodium transport across tight epithelia. *In* Ion Transport by Epithelia. S. G. Schultz, editor. Raven Press, New York. 93–107.

36. Lewis, S. A., N. K. Wills, and D. C. Eaton. 1978. Basolateral membrane potential of a tight epithelium: ionic diffusion and electrogenic pumps. *J. Membr. Biol.* 41:117–148.

37. Lorenzen, M., H. Sackin, C. O. Lee, and E. E. Windhager. 1981. Intracellular Na^+ activity, basolateral membrane potential and transepithelial voltage in isolated perfused proximal tubules of *Necturus* kidney. *Fed. Proc.* 40:394. (Abstr.)

38. Machen, T. E., and J. M. Diamond. 1969. An estimate of the salt concentration in the lateral intercellular spaces of rabbit gall bladder during maximal fluid transport. *J. Membr. Biol.* 1:194–213.

39. Maunsbach, A., and E. L. Boulpaep. 1983. Quantitative ultrastructure and functional correlates in proximal tubules of *Ambystoma* and *Necturus*. *Am. J. Physiol.* In press.

40. Mullins, L. J., and M. Z. Awad. 1965. The control of the membrane potential of muscle fibers by the sodium pump. *J. Gen. Physiol.* 48:761–775.

41. Nagel, W. 1980. Rheogenic sodium transport in a tight epithelium, the amphibian skin. *J. Physiol. (Lond.).* 302:281–295.

42. Nielsen, R. 1979. A 3 to 2 coupling of the Na-K pump responsible for the transepithelial Na transport in frog skin disclosed by the effect of Ba. *Acta Physiol. Scand.* 107:189–191.

43. Proverbio, F., and G. Whittembury. 1975. Cell electrical potentials during enhanced sodium extrusion in guinea-pig kidney cortex slices. *J. Physiol. (Lond.)* 250:559–578.

44. Rose, R. C., and D. L. Nahrwold. 1976. Electrolyte transport by gall bladders of rabbit and guinea pig: effect of amphotericin B and evidence of rheogenic Na transport. *J. Membr. Biol.* 29:1–22.

45. Rose, R. C., D. L. Nahrwold, and M. J. Koch. 1977. Electrical potential profile in rabbit ileum: role of rheogenic Na transport. *Am. J. Physiol.* 232:E5–E12.

46. Reuss, L., E. Bello-Reuss, and T. P. Grady. 1979. Effects of ouabain on fluid transport and electrical properties of *Necturus* gall bladder: evidence in favor of a neutral basolateral sodium transport mechanism. *J. Gen. Physiol.* 73:385–402.

47. Reuss, L., and S. A. Weinman. 1979. Intracellular ionic activities and transmembrane electrochemical potential differences in gall bladder epithelium. *J. Membr. Biol.* 49:345–362.
48. Sackin, H., W. F. Boron, and E. L. Boulpaep. 1981. Intracellular sodium activity in *Ambystoma* renal proximal tubule. *Kidney Int.* 19:255. (Abstr.)
49. Sackin, H., and E. L. Boulpaep. 1975. Models for coupling salt and water transport: proximal tubular reabsorption in *Necturus* kidney. *J. Gen. Physiol.* 66:671–732.
50. Sackin, H., and E. L. Boulpaep. 1981. Isolated perfused salamander proximal tubule: methods, electrophysiology, and transport. *Am. J. Physiol.* 241:F39–F52.
51. Sackin, H., and E. L. Boulpaep. 1981. Isolated perfused salamander proximal tubule. II. Monovalent ion replacement and rheogenic transport. *Am. J. Physiol.* 241:F540–F555.
52. Sackin, H., A. B. Maunsbach, and E. L. Boulpaep. 1982. Correlation between basolateral membrane electrical resistance and ultrastructure in isolated perfused renal proximal tubules. *Kidney Int.* 21:286. (Abstr.)
53. Schwartz, T. L. 1971. Direct effects on the membrane potential due to "pumps" that transfer no net charge. *Biophys. J.* 11:944–960.
54. Spring, K. R., and A.-C. Ericson. 1982. Epithelial cell volume modulation and regulation. *J. Membr. Biol.* 69:167–176.
55. Spring, K. R., and G. Kumura. 1978. Chloride reabsorption by renal proximal tubules of *Necturus*. *J. Membr. Biol.* 38:233–254.
56. Stirling, E. S. 1972. Radioautographic localization of sodium pump sites in rabbit intestine. *J. Cell Biol.* 53:704–714.
57. Taylor, R. E. 1952. The distribution of membrane current in nerve with longitudinal linearly increasing applied current. *Bull. Math. Biophys.* 14:265–292.
58. Thomas, R. C. 1972. Electrogenic sodium pump in nerve and muscle cells. *Physiol. Rev.* 52:563–594.
59. Thomas, R. C. 1979. Construction of solid-state Na^+ and K^+ sensitive microelectrodes. *In* Ion-Sensitive Intracellular Microelectrodes. Academic Press, Inc., New York. 45–49.
60. Whittembury, G. 1974. Cellular and paracellular mechanisms in sodium transport in the proximal tubule. *Proc. 5th Int. Congr. Nephrol.* 2:18–28.
61. Wills, N. K., and S. A. Lewis. 1980. Intracellular Na^+ activity as a function of Na^+ transport rate across a tight epithelium. *Biophys. J.* 30:181–186.
62. Wills, N. K., S. A. Lewis, and D. C. Eaton. 1979. Active and passive properties of rabbit descending colon: a microelectrode and nystatin study. *J. Membr. Biol.* 45:81–108.
63. Windhager, E. E., E. L. Boulpaep, and G. Giebisch. 1966. Electrophysiological studies on single nephrons. *Proc. 3rd Int. Cong. Nephrol.* 1:35–47.